

## Structure–Activity Relationships in Gold Nanoparticle Dimers and Trimers for Surface-Enhanced Raman Spectroscopy

Kristin L. Wustholz,<sup>†</sup> Anne-Isabelle Henry,<sup>†</sup> Jeffrey M. McMahon,<sup>†</sup>  
R. Griffith Freeman,<sup>‡</sup> Nicholas Valley,<sup>†</sup> Marcelo E. Piotti,<sup>‡</sup> Michael J. Natan,<sup>‡</sup>  
George C. Schatz,<sup>†</sup> and Richard P. Van Duyne<sup>\*†</sup>

Department of Chemistry, Northwestern University, 2145 Sheridan Road, Evanston,  
Illinois 60208, and Oxonica Materials Incorporated, 325 East Middlefield Road, Mountain View,  
California 94043

Received May 14, 2010; E-mail: vanduyne@northwestern.edu

**Abstract:** Understanding the detailed relationship between nanoparticle structure and activity remains a significant challenge for the field of surface-enhanced Raman spectroscopy. To this end, the structural and optical properties of individual plasmonic nanoantennas comprised of Au nanoparticle assemblies that are coated with organic reporter molecules and encapsulated by a SiO<sub>2</sub> shell have been determined using correlated transmission electron microscopy (TEM), dark-field Rayleigh scattering microscopy, surface-enhanced Raman scattering (SERS) microscopy, and finite element method (FEM) calculations. The distribution of SERS enhancement factors (EFs) for a structurally and optically diverse set of nanoantennas is remarkably narrow. For a collection of 30 individual nanoantennas ranging from dimers to heptamers, the EFs vary by less than 2 orders of magnitude. Furthermore, the EFs for the hot-spot-containing nanoparticles are uncorrelated to aggregation state and localized surface plasmon resonance (LSPR) wavelength but are crucially dependent on the size of the interparticle gap. This study demonstrates that the creation of hot spots, where two particles are in subnanometer proximity or have coalesced to form crevices, is paramount to achieving maximum SERS enhancements.

### Introduction

The Raman scattering from molecules adsorbed to nanostructured metal surfaces can be enhanced by a factor of a million or more as compared to the signal from free molecules in a process known as surface-enhanced Raman scattering (SERS).<sup>1</sup> Owing to these remarkable signal enhancements, considerable effort has been devoted to the development of chemical and biological sensors based on SERS,<sup>2,3</sup> and detection of single molecules on Ag nanoparticle aggregates has been demonstrated.<sup>4,5</sup> As it is currently understood, single-molecule SERS (SMSERS) requires substrates containing “hot spots”, regions of high electromagnetic (EM) enhancement in the junctions between metallic nanoparticles.<sup>6,7</sup> However, the relationship of SERS enhancement factors (EFs) to the structural and optical properties of hot-spot-containing substrates remains elusive.

SERS enhancement can originate from resonance Raman, chemical, and EM contributions.<sup>8–10</sup> For the case of a non-resonant adsorbate, EM effects that result from exciting the localized surface plasmon resonance (LSPR) of the substrate will dominate.<sup>3,9,11</sup> For example, ensemble-averaged studies of benzenethiol adsorbed to arrays of isolated Ag nanoparticles demonstrated that SERS enhancement is largest when the LSPR is between the laser-excitation and Stokes-shifted frequencies.<sup>12</sup> Furthermore, the distance between plasmonic structures is known to play an important role in SERS<sup>6,13,14</sup> as well as in surface-enhanced fluorescence.<sup>15–18</sup> Yet, the detailed relationships among structure, plasmon resonance, and SERS enhancement for hot-spot-containing nanostructures have not been

<sup>†</sup> Northwestern University.

<sup>‡</sup> Oxonica Materials Inc.

- (1) Jeanmaire, D. L.; Van Duyne, R. P. *J. Electroanal. Chem.* **1977**, *84*, 1.
- (2) Camden, J. P.; Dieringer, J. A.; Zhao, J.; Van Duyne, R. P. *Acc. Chem. Res.* **2008**, *41*, 1653.
- (3) Stiles, P. L.; Dieringer, J. A.; Shah, N. C.; Van Duyne, R. R. *Annu. Rev. Anal. Chem.* **2008**, *1*, 601.
- (4) Kneipp, K.; Wang, Y.; Kneipp, H.; Perelman, L. T.; Itzkan, I.; Dasari, R.; Feld, M. S. *Phys. Rev. Lett.* **1997**, *78*, 1667.
- (5) Nie, S. M.; Emory, S. R. *Science* **1997**, *275*, 1102.
- (6) Camden, J. P.; Dieringer, J. A.; Wang, Y. M.; Masiello, D. J.; Marks, L. D.; Schatz, G. C.; Van Duyne, R. P. *J. Am. Chem. Soc.* **2008**, *130*, 12616.
- (7) Michaels, A. M.; Jiang, J.; Brus, L. *J. Phys. Chem. B* **2000**, *104*, 11965.

- (8) Morton, S. M.; Jensen, L. *J. Am. Chem. Soc.* **2009**, *131*, 4090.
- (9) Gersten, J.; Nitzan, A. *J. Chem. Phys.* **1980**, *73*, 3023.
- (10) Dieringer, J. A.; Wustholz, K. L.; Masiello, D. J.; Camden, J. P.; Kleinman, S. L.; Schatz, G. C.; Van Duyne, R. P. *J. Am. Chem. Soc.* **2009**, *131*, 849.
- (11) Laurent, G.; Felidj, N.; Grand, J.; Aubard, J.; Levi, G.; Hohenau, A.; Ausseneegg, F. R.; Krenn, J. R. *Phys. Rev. B* **2006**, *73*, 5.
- (12) McFarland, A. D.; Young, M. A.; Dieringer, J. A.; Van Duyne, R. P. *J. Phys. Chem. B* **2005**, *109*, 11279.
- (13) McMahon, J. M.; Henry, A. I.; Wustholz, K. L.; Natan, M. J.; Freeman, R. G.; Van Duyne, R. P.; Schatz, G. C. *Anal. Bioanal. Chem.* **2009**, *394*, 1819.
- (14) Danckwerts, M.; Novotny, L. *Phys. Rev. Lett.* **2007**, *98*, 4.
- (15) Kinkhabwala, A.; Yu, Z. F.; Fan, S. H.; Avlasevich, Y.; Mullen, K.; Moerner, W. E. *Nat. Photonics* **2009**, *3*, 654.
- (16) Kuhn, S.; Hakanson, U.; Rogobete, L.; Sandoghdar, V. *Phys. Rev. Lett.* **2006**, *97*, 4.
- (17) Muskens, O. L.; Giannini, V.; Sanchez-Gil, J. A.; Rivas, J. G. *Nano Lett.* **2007**, *7*, 2871.
- (18) Anger, P.; Bharadwaj, P.; Novotny, L. *Phys. Rev. Lett.* **2006**, *96*, 4.

thoroughly addressed. Measuring the structure–activity relationship in SMSERS-active substrates is problematic for several reasons. First, the vast majority of SERS measurements are performed in bulk using thousands to millions of nanoparticles, and much information is lost in the averaging over an ensemble.<sup>11,19</sup> Furthermore, SMSERS substrates are polydisperse Ag nanoparticles that are randomly aggregated using salt; the heterogeneity and irreproducibility of these nanostructures makes it difficult to perform systematic investigations. Although previous studies showed no evidence of a correlation between SMSERS intensity and the extinction properties of colloidal aggregates,<sup>20</sup> these investigations are complicated by the fact that the nanoparticle structure as well as the location of the single molecule on the substrate are not precisely known. Recently, correlated atomic force microscopy (AFM), SERS, and Rayleigh scattering measurements were used to explore the SERS activity of individual Au nanoparticles, but the resolution of AFM is prohibitive, and well-defined structure–activity relationships were not established in these studies.<sup>21,22</sup>

Our approach is to study individual “SERS nanoantennas”, SiO<sub>2</sub>-encapsulated Au nanoparticles to which Raman-active molecules have been adsorbed.<sup>23–25</sup> Prior to glass coating, the spherical, monodisperse metallic cores are assembled to form well-defined and reproducible structures such as dimers, trimers, and higher-order aggregates. In this work, the nanoantennas are functionalized with a Raman reporter molecule (2-(4-pyridyl)-2-cyano-1-(4-ethynylphenyl)ethylene) (termed PCEPE), which according to density functional theory (DFT) possesses a large Raman cross-section of  $2.47 \times 10^{-28}$  cm<sup>2</sup>/sr and is therefore convenient for study. Encapsulation in a SiO<sub>2</sub> shell provides multiyear shelf stability, enhanced photostability, and a well-defined external dielectric environment. As prepared from solution, the nanoantennas exist in a variety of aggregation states from monomers to octamers, which can be enriched using field flow fractionation.<sup>26</sup> Because of the composition and stability of the SERS nanoantennas, it is possible to address several outstanding questions about the nature of enhancement in substrates containing hot spots. For example, what structural features lead to maximum enhancement? Do gaps between metal nanoparticles as well as crevices that form in the junction of fused nanoparticles provide for the high enhancements associated with SMSERS (i.e.,  $\geq 10^8$ )?<sup>10</sup> What is the role of the LSPR wavelength in determining EF? In this study, correlated TEM, dark-field Rayleigh scattering microscopy, SERS microscopy, and finite element method (FEM) calculations are performed

at the single-nanoantenna level in order to address these outstanding questions.

## Materials and Methods

**Sample Preparation.** PCEPE was prepared by Knoevenagel condensation of 4-pyridyl acetonitrile and 4-ethynyl benzaldehyde. It was purified by recrystallization from ethanol/water. The synthesis of SERS nanoantennas was performed according to previous work.<sup>25</sup> In order to reduce structural diversity within the sample, sedimentation field flow fractionation (PostNova Analytics, S-101) was employed. A 100  $\mu$ L amount of material was injected onto the column at a concentration of  $\sim 9 \times 10^{14}$  particles/L, and deionized water was used in the separation. Beginning 5 min after injection fractions were collected over 5 min intervals for 30 min. Fractions were centrifuged at 3200 rpm for 40 min and then resuspended in 10.0 mL of deionized H<sub>2</sub>O.

**TEM Measurements.** SERS nanoantennas were deposited on a 300-mesh TEM grid (Ted Pella Formvar/Carbon type B) by drop casting 10  $\mu$ L of the aqueous solution of nanoantennas. The samples were dried in air. TEM images were obtained on a Jeol JEM-2100F fast TEM microscope operating at 200 kV. Values of  $d_{\text{gap}}$  were investigated in HRTEM by tilting the sample (double-tilt holder Jeol 31630) so that the gap region was observed at normal incidence.

**Optical Microscopy.** The TEM grid containing nanoantennas was placed on a clean glass coverslip (Fisher Scientific) atop an inverted microscope (Nikon TE300) equipped with a dark-field condenser (numerical aperture, NA = 0.7–0.95) and a variable NA 100 $\times$  oil-immersion objective (Nikon Plan Fluor, NA = 0.5–1.3) set to NA = 0.5 to collect Rayleigh scattering from the nanoantennas following white-light illumination. The dark-field Rayleigh scattering, termed LSPR throughout the manuscript, was sent to a 1/3 m monochromator (Acton 300i) containing a low-dispersion grating blazed at 500 nm (150 groove/mm) and detected by a LN<sub>2</sub>-cooled CCD detector (Princeton Instruments, Spec-10 400B). A wide-field ( $\sim 200 \mu\text{m}^2$ ) LSPR image was collected in order to identify the unique relative positions of the nanoantennas for correlation to TEM. LSPR spectra of individual nanoantennas were obtained by centering each diffraction-limited spot at the entrance slit of the spectrograph. The LSPR measurements were corrected by the spectral lamp profile.

Normal Raman and SERS microscopy were performed using 632.8 nm excitation from a HeNe laser (Research Electro-Optics, 17 mW) that was sent through a notch filter (Semrock, NF03-633  $\times 10^{-25}$ ) and focused to a diffraction-limited spot using a 50 $\times$  objective (Nikon Plan Fluor, NA = 0.55). Raman scattering from the sample was sent through an edge filter (Semrock, LL01-633-25) and a 1200 grooves/mm grating blazed at 500 nm and detected by the LN<sub>2</sub>-cooled CCD detector. Typical laser powers and acquisition times for SERS measurements were 0.1 mW and 30 s, respectively. Normal Raman measurements were performed on a 36.5 mM solution of PCEPE in ethanol.

**Enhancement Factor Calculation.** The EF of individual nanoantennas was determined by computing the ratio of SERS to normal Raman scattering (NRS) of PCEPE using the following expression

$$\text{EF} = \frac{(I_{\text{SERS}}/N_{\text{SERS}})}{(I_{\text{NRS}}/N_{\text{NRS}})} \quad (1)$$

where  $I_{\text{SERS}}$  and  $I_{\text{NRS}}$  correspond to the integrated SERS and NRS intensities, respectively, normalized for acquisition time and laser power.  $I_{\text{NRS}}$  was determined to be  $5.7 \text{ cts mW}^{-1} \text{ s}^{-1}$ .  $N_{\text{SERS}}$  and  $N_{\text{NRS}}$  are the number of molecules probed in the SERS and NRS measurements.  $N_{\text{SERS}}$  is established by the conditions of nanoantenna synthesis. Briefly, 300  $\mu$ L of a 0.1 mM PCEPE solution was added to 100 mL of Au nanoparticles (i.e.,  $\sim 1.4 \times 10^{10}$  particles/mL). Therefore, there are approximately 13 300 PCEPE molecules per monomer, assuming 100% adsorption. Since  $N_{\text{SERS}}$  is an upper-

- (19) Chen, G.; Wang, Y.; Yang, M. X.; Xu, J.; Goh, S. J.; Pan, M.; Chen, H. Y. *J. Am. Chem. Soc.* **2010**, *132*, 3644.
- (20) Michaels, A. M.; Nirmal, M.; Brus, L. E. *J. Am. Chem. Soc.* **1999**, *121*, 9932.
- (21) Tay, L.-L.; Hulse, J.; Kennedy, D.; Pezacki, J. P. *J. Phys. Chem. C* **2010**, *114*, 7356.
- (22) Talley, C. E.; Jackson, J. B.; Oubre, C.; Grady, N. K.; Hollars, C. W.; Lane, S. M.; Huser, T. R.; Nordlander, P.; Halas, N. J. *Nano Lett.* **2005**, *5*, 1569.
- (23) Sha, M. Y.; Xu, H. X.; Natan, M. J.; Cromer, R. *J. Am. Chem. Soc.* **2008**, *130*, 17214.
- (24) Freeman, R. G.; Grabar, K. C.; Allison, K. J.; Bright, R. M.; Davis, J. A.; Guthrie, A. P.; Hommer, M. B.; Jackson, M. A.; Smith, P. C.; Walter, D. G.; Natan, M. J. *Science* **1995**, *267*, 1629.
- (25) Mulvaney, S. P.; Musick, M. D.; Keating, C. D.; Natan, M. J. *Langmuir* **2003**, *19*, 4784.
- (26) Giddings, J. C.; Yang, F. J. F.; Myers, M. N. *Science* **1976**, *193*, 1244.

bound estimate, the calculated EFs are lower-bound estimates. Furthermore, the EFs are experimentally relevant, nanoantenna-averaged values and not maximum enhancements, which others have attempted to calculate by estimating the number of molecules in the hot spot.  $N_{\text{NRS}}$  was determined to be  $7 \times 10^9$  according to  $N_{\text{NRS}} = C_{\text{NRS}} V_{\text{probe}}$ , where  $C_{\text{NRS}}$  is the concentration of PCEPE in solution (i.e.,  $2.2 \times 10^{19}$  molecules/mL) and  $V_{\text{probe}}$  is the probe volume of the laser. Scanning knife edge measurements on Si were used to determine  $V_{\text{probe}}$ , which is approximated as the volume of an ellipsoid,  $V_{\text{probe}} = 4/3\pi r_x r_y r_z$ , where  $r$  is the radius of the laser spot in the  $x$ ,  $y$ , and  $z$  directions.  $r_x$ ,  $r_y$ , and  $r_z$  were determined to be 2.2, 1.5, and 22  $\mu\text{m}$  respectively. For the L-shaped trimer,  $N_{\text{SERS}}$  is  $4.0 \times 10^4$  and  $I_{\text{SERS}}$  is  $5.9 \times 10^3$  cts  $\text{mW}^{-1} \text{s}^{-1}$ , leading to an overall EF expression

$$\text{EF} = \frac{(5.9 \times 10^3 / 4.0 \times 10^4)}{(5.7 \times 10^0 / 7.0 \times 10^9)} = 1.8 \times 10^8 \quad (2)$$

The standard deviation of the calculated EFs was determined to be 5% based on multiple NRS measurements. However, the most significant source of uncertainty originates from day-to-day variations in the laser spot size with alignment, which impact  $N_{\text{NRS}}$ . Therefore,  $V_{\text{probe}}$  was measured during each experiment.

**DFT Calculations.** The NRS expected for PCEPE was calculated using DFT [local version of the Amsterdam density functional (ADF) code ADF2009.01, SCM, Theoretical Chemistry, Vrije Universiteit, Amsterdam, The Netherlands]. Full geometry optimization and frequency calculations were completed using the Becke–Perdew (BP86) XC-potential and a triple- $\xi$ -polarized Slater-type (TZP) basis set. For calculation of polarizabilities, the hybrid B3LYP functional and TZP basis set were used. Polarizabilities were calculated at zero frequency and within the adiabatic local density approximation using the AOResponse module within ADF. Polarizability derivatives were calculated with numerical three-point differentiation with respect to the normal mode vibration displacements. Absolute Raman intensities were given as the differential Raman cross-section for Stokes scattering assuming an experimental setup with a 90° scattering angle and perpendicular plane-polarized light calculated using the expression

$$\frac{d\sigma}{d\Omega} = \frac{h}{8\varepsilon_0^2 c \nu_k} (\nu_{\text{in}} - \nu_k)^4 \frac{(45\alpha'_k + 7\gamma'_k)}{45(1 - \exp(-hcv_k/k_B T))} \quad (3)$$

where  $\alpha'_k$  and  $\gamma'_k$  are the isotropic and anisotropic polarizability derivatives with respect to the  $k$ th vibrational mode,  $\nu_k$  is the frequency of the mode  $k$ , and  $\nu_{\text{in}}$  is the incident light frequency. A wavelength of 632.8 nm was assumed for the incident light for the Raman cross-section calculations. Each peak in the vibrational spectrum was broadened using a 20  $\text{cm}^{-1}$  wide Lorentzian function. The most intense normal Raman mode at 1562  $\text{cm}^{-1}$  corresponds to benzene ring vibrations that are coupled to the central ethylene bond.

**FEM Calculations.** The FEM was used for our three-dimensional electrodynamics calculations. Further details of FEM and the method used for our 2D calculations can be found elsewhere.<sup>13,27</sup> For 3D calculations, we solved the vector wave equation for the electric field

$$\nabla \times \left( \frac{1}{\mu_r} \nabla \times \vec{E} \right) - k_0^2 \varepsilon_r \vec{E} = 0 \quad (4)$$

in SI units, where  $\mu_r$  is the relative permeability,  $\varepsilon_r$  is the relative permittivity,  $\vec{E}$  is the electric field, and  $k_0 = 2\pi/\lambda_0$  is the incident wavevector magnitude, where  $\lambda_0$  is the incident wavelength. In order

to model open-region scattering from the nanoantennas, we also considered the Sommerfeld radiation condition<sup>27</sup>

$$\lim_{r \rightarrow \infty} \{ r [\nabla \times \vec{E} + ik_0 \hat{r} \vec{E}] \} = 0 \quad (5)$$

In order to solve eq 4, subject to eq 5, a standard Ritz variational method was used. The functional for these equations (the latter approximated to first order) is

$$F(\vec{E}) = \frac{1}{2} \int_V dV \left[ \frac{1}{\mu_r} (\nabla \times \vec{E}) \cdot (\nabla \times \vec{E}) - k_0^2 \varepsilon_r \vec{E} \cdot \vec{E} \right] + \oint_S dS \left[ \frac{ik_0}{2} (\hat{r} \times \vec{E}) \cdot (\hat{r} \times \vec{E}) + \vec{E} \cdot \vec{U}_{\text{inc}} \right] \quad (6)$$

where  $\vec{U}_{\text{inc}} = \hat{r} \times \nabla \times \vec{E}_{\text{inc}} + ik_0 \hat{r} \times \hat{r} \times \vec{E}_{\text{inc}}$ , with  $\vec{E}_{\text{inc}}$  being the incident field, which for our calculations was a plane wave. The unknown  $\vec{E}$  can be found from the stationary point of  $F(\vec{E})$ , which we found using FEM. This was done by discretizing a domain (with subdomains termed elements) and finding the stationary point with respect to each using a basis function expansion (over each element) for  $\vec{E}$ . Care was taken such that the appropriate boundary conditions on the interfaces between connecting elements (continuity of the tangential component of the field) was satisfied and eq 4 would remain valid over the entire domain. In this work, tetrahedral elements were used for the volume integral, which implies triangular surface elements. In addition, vector basis functions constructed from Whitney edge elements with the curl of  $\vec{E}$  complete to a polynomial of order 1 were used to approximate  $\vec{E}$ .<sup>28</sup>

The trimer was modeled by three 100 nm diameter Au spherical particles with 50 nm thick spherical  $\text{SiO}_2$  shells. The structure was placed at the origin, and the computational domain was extended to 400 nm, sufficiently far so that eq 5 is approximately satisfied. Tetrahedral elements of the trimer were limited to a maximum of 40 nm<sup>3</sup>, except for the junction and outer element regions, which were limited to 10 and 90 nm<sup>3</sup>, respectively. The dielectric function of Au was modeled after empirically inferred dielectric data using a Drude plus two Lorentz pole function with parameters.<sup>29</sup> The dielectric function of  $\text{SiO}_2$  was taken to be constant at 2.25. Cross sections were calculated using volume integral equations, 3D analogs of those outlined elsewhere.<sup>13</sup> The maximum enhancement of the nanoantenna is defined as the single point of highest intensity. The average enhancement was obtained by evaluating the intensity at a number of points, 0.1 nm from the nanoantenna surface, and computing the average.

## Results and Discussion

TEM was used to characterize the structures of fractionated SERS nanoantennas. The first and second fractions consist almost entirely of monomers. From TEM measurements of 89 individual nanoantennas, the distribution of aggregation states in the third fraction was determined to be 52% monomers, 10% dimers, 21% trimers, 13% tetramers, and 3% pentamers or higher-order aggregates. Accordingly, correlated TEM, SERS, and LSPR measurements were performed on nanoantennas from this fraction to establish the structure–activity relationship in simple geometries such as dimers and trimers. The Au cores and  $\text{SiO}_2$  shells are remarkably monodisperse, with average diameters of  $97.1 \pm 1.5$  and  $48.0 \pm 0.6$  nm, respectively, where the error corresponds to the standard deviation of the mean (Figure 1a). The distribution of 60 single-nanoantenna LSPR maxima and the corresponding ensemble-averaged data are presented in Figure 1b. The single-nanoantenna LSPR distribu-

(27) Jin, J. *The Finite Element Method in Electromagnetics*; John Wiley and Sons: New York, 2002.

(28) Graglia, R. D.; Wilton, D. R.; Peterson, A. F. *IEEE Trans. Antennas Propag.* **1997**, 45, 329.

(29) Johnson, P. B.; Christy, R. W. *Phys. Rev. B* **1972**, 6, 4370.

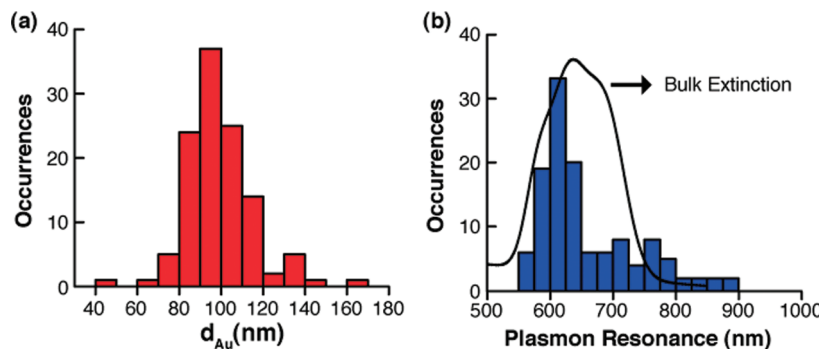


**Figure 1.** Structural and optical characterization of 60 SERS nanoantennas from fractions 1–3. (a) Distribution of  $d_{\text{Au}}$  obtained from TEM measurements. (b) Corresponding histogram of 123 LSPR maxima is consistent with the ensemble-averaged extinction spectrum measured on glass (black curve).

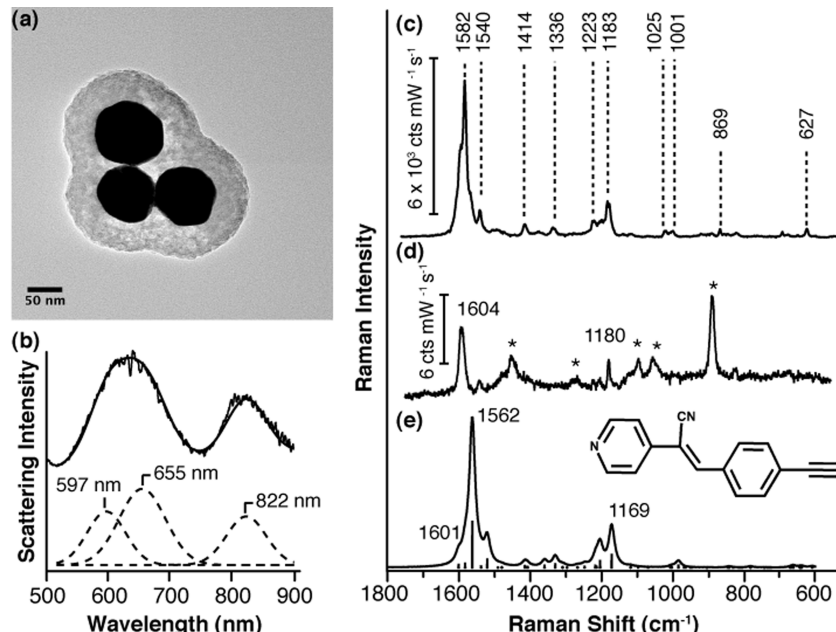


**Figure 2.** Correlated structural and optical characterization of an individual SERS nanoantenna. (a) Transmission electron micrograph of an L-shaped trimer nanoantenna comprised of three Au cores functionalized with PCEPE (structure shown) and encapsulated in a SiO<sub>2</sub> shell. (b) Corresponding LSPR spectrum of the L-shaped trimer obtained by dark-field Rayleigh scattering microscopy fit to a sum of three Gaussian functions (dashed lines), and (c) SERS spectrum following 632.8 nm excitation from a HeNe laser at low power (0.1 mW) and a 30 s acquisition time to prevent molecular photobleaching. Prominent vibrational modes are highlighted. (d) Raman spectrum of 36.5 mM PCEPE in ethanol (solvent peaks are marked by asterisks). (e) Raman spectrum of PCEPE calculated using DFT.

tion is consistent with the ensemble-averaged measurement and exhibits a maximum near the laser excitation wavelength at 632.8 nm. Furthermore, since the dielectric environment for all nanoantennas is equivalent, the broad distribution of LSPR maxima (i.e., ranging >300 nm) is consistent with the existence of diverse structural properties within the sample.

A transmission electron micrograph of a trimer nanoantenna containing three Au cores in an “L” shape is shown in Figure 2a. Two junctions are present, where Au cores in the vertically oriented dimer appear to be separated by an interparticle gap size ( $d_{\text{gap}}$ ) of <1 nm, and the horizontally oriented dimer seems to be coalesced ( $d_{\text{gap}} < 0$ ). In order to measure the optical properties of this nanoantenna we used pattern matching of TEM imaging and wide-field LSPR microscopy, a recently developed high-throughput and reliable technique.<sup>6,30</sup> The dark-field Rayleigh scattering spectrum of the L-shaped trimer contains three

peaks (Figure 2b), corresponding to dipolar and multipolar LSPRs.<sup>31</sup> By focusing a laser to a diffraction-limited spot at the location of the dark-field Rayleigh scattering, the SERS spectrum of the adsorbed PCEPE molecules was obtained (Figure 2c). In this case, the single-nanoantenna SERS signal (i.e.,  $5.9 \times 10^3$  counts  $\text{mW}^{-1} \text{s}^{-1}$  for the  $1582 \text{ cm}^{-1}$  mode) following 632.8 nm laser excitation originates from only ~40 000 PCEPE molecules. The SERS spectrum is consistent with the measured and DFT-calculated normal Raman spectrum of PCEPE (Figures 2d and 2e, respectively), although modest deviations between the Raman and SERS vibrational frequencies are observed due to local environmental effects when molecules are adsorbed to metal surfaces.<sup>32</sup> The Raman cross-section of PCEPE was determined by DFT calculations to be  $2.47 \times 10^{-28} \text{ cm}^2/\text{sr}$ . The EF of the L-shaped nanoantenna for the vibrations

(30) Wang, Y.; Eswaramoorthy, S. K.; Sherry, L. J.; Dieringer, J. A.; Camden, J. P.; Schatz, G. C.; Van Duyne, R. P.; Marks, L. D. *Ultramicroscopy* **2009**, *109*, 1110.

(31) Sung, J. H.; Sukharev, M.; Hicks, E. M.; Van Duyne, R. P.; Seideman, T.; Spears, K. G. *J. Phys. Chem. C* **2008**, *112*, 3252.  
(32) Zhao, J.; Jensen, L.; Sung, J. H.; Zou, S. L.; Schatz, G. C.; Van Duyne, R. P. *J. Am. Chem. Soc.* **2007**, *129*, 7647.

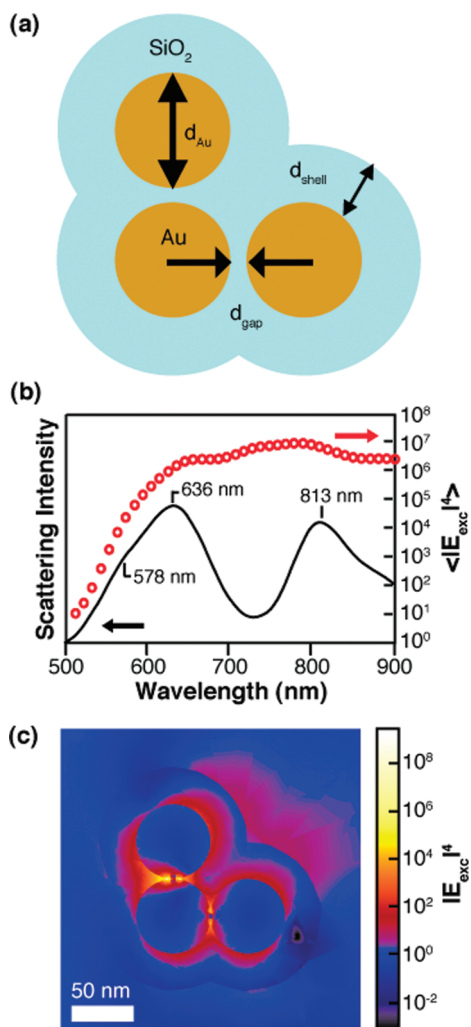


**Figure 3.** FEM calculations of L-shaped nanoantenna. (a)  $d_{\text{Au}}$  and  $d_{\text{shell}}$  were set to 100 and 50 nm, respectively, consistent with TEM measurements. (b) Best fit to the experimental scattering spectrum (solid line) was obtained using a value for  $d_{\text{gap}}$  of  $-0.35$  nm, corresponding to modestly coalesced cores. The calculated  $\langle |E_{\text{exc}}|^4 \rangle$  as a function of excitation wavelength (red open circles) demonstrates that the enhancement is relatively constant from about 600 to 900 nm. (c) Image of  $|E_{632.8 \text{ nm}}|^4$  for the L-shaped nanoantenna demonstrating two hot spots located at the junctions between nanoparticles. The maximum and average EFs of the nanoantenna are  $3.2 \times 10^9$  and  $1.1 \times 10^6$ , respectively.

at  $1582$  and  $1183 \text{ cm}^{-1}$  were determined to be  $1.8 \times 10^8$  and  $2.0 \times 10^8$ , respectively. Since the EFs are relatively independent of vibrational frequency and the mode at  $1582 \text{ cm}^{-1}$  provided the highest signal-to-noise ratio, this mode is used hereafter to determine EF.

The geometric parameters of the L-shaped nanoantenna obtained from TEM measurements were used for computational modeling via the FEM (Figure 3a). As compared to traditional grid-based approaches such as the finite-difference time-domain method, FEM is more accurate for complex structures, since it allows for exact geometrical modeling. Accordingly, the diameters of the Au cores ( $d_{\text{Au}}$ ) and  $\text{SiO}_2$  shell ( $d_{\text{shell}}$ ) were set to 100 and 50 nm, respectively. In order to best reproduce the experimental LSPR spectrum, interparticle gap sizes were varied from  $-2$  (where the negative distance is used to denote coalesced cores) to 2 nm. Best fit to the data corresponded to modestly coalesced cores with  $d_{\text{gap}}$  equal to  $-0.35$  nm. The resulting scattering cross-section as a function of wavelength

(Figure 3b) exhibited three maxima at 578, 636, and 813 nm. Consistent with the calculated result, the experimental spectrum shown in Figure 2b was fit to three Gaussian functions centered at 597, 655, and 822 nm. The corresponding antenna-averaged EM enhancement ( $\langle |E_{\text{exc}}|^4 \rangle$ ), which is evaluated 0.1 nm from the nanoantenna surface, was determined as a function of excitation wavelength (Figure 3b). Similar to previous computational studies of Au dimers,<sup>17</sup>  $\langle |E_{\text{exc}}|^4 \rangle$  is relatively constant between 600 and 900 nm, varying by less than an order of magnitude in this region. An intensity profile of the EM enhancement at 632.8 nm,  $|E_{632.8 \text{ nm}}|^4$ , is presented in Figure 3c. It is seen that the L-shaped trimer truly acts as an antenna by concentrating the fields at hot spots between Au cores to provide a maximum enhancement of  $3.2 \times 10^9$ . The nanoantenna-averaged EF was determined to be  $1.1 \times 10^6$ , which underestimates the experimentally obtained value by approximately 2 orders of magnitude. Surface roughness and chemical enhancements, both not accounted for in the calculations, are expected to increase the total SERS enhancement.<sup>8,33,34</sup>

Correlated structural, optical, and computational studies of the L-shaped nanoantenna demonstrate that the EM enhancement is localized in hot spots and that the EF is relatively wavelength independent. These observations suggest that the laser excitation wavelength need not match the plasmon resonance wavelength in order to achieve high EM enhancement. What, then, is the most important physical or optical parameter for establishing high EFs in hot-spot-containing nanoparticles? In order to address this question it is necessary to perform correlated measurements of many nanoantennas with various structural and optical characteristics. To this end, correlated TEM, LSPR, and SERS measurements were performed on 67 individual nanoantennas. SERS signal was not observed for monomers ( $\text{EF} \leq 10^4$ ) under the experimental conditions, consistent with a reduction to EM enhancement for isolated nanoparticles.<sup>7,13,21,35,36</sup> For the remaining 33 dimers and higher-order aggregates, SERS signal was observed for 91%, or 30 out of 33, of nanoantennas. TEM measurements revealed that the interparticle gaps in the small population of “dim” nanoantennas were sufficiently small (i.e.,  $< 1$  nm) to support the observation of SERS. As a result, we attributed these observations to a lack of planarity of the TEM grid, which caused problems focusing the laser to the sample.

Examples of correlated measurements of single nanoantennas are shown in Figure 4. Comparing the structures, LSPR spectra, and corresponding EFs of these nanoantennas provides several important insights. First, diverse nanostructures give rise to extremely different LSPR spectra as expected.<sup>37,38</sup> For example, the nanoantenna dimer and trimer in Figure 4a and 4d, respectively, have significantly different plasmon resonances. Yet, the dimers in Figure 4a and 4b have nearly identical structures (i.e.,  $d_{\text{Au}}$ ,  $d_{\text{shell}}$ , geometry) but diverse LSPR spectra, suggesting that the aggregation state and geometry of the nanoantennas are not solely responsible for determining LSPR. Recent computational studies of Au dimers suggest that the extinction properties of nanoantennas are highly dependent on

- (33) Aikens, C. M.; Schatz, G. C. *J. Phys. Chem. A* **2006**, *110*, 13317.
- (34) Laor, U.; Schatz, G. C. *Chem. Phys. Lett.* **1981**, *82*, 566.
- (35) Lim, D. K.; Jeon, K. S.; Kim, H. M.; Nam, J. M.; Suh, Y. D. *Nat. Mater.* **2010**, *9*, 60.
- (36) Metiu, H.; Das, P. *Annu. Rev. Phys. Chem.* **1984**, *35*, 507.
- (37) Zhao, L. L.; Kelly, K. L.; Schatz, G. C. *J. Phys. Chem. B* **2003**, *107*, 7343.
- (38) Willets, K. A.; Van Duyne, R. P. *Annu. Rev. Phys. Chem.* **2007**, *58*, 267.

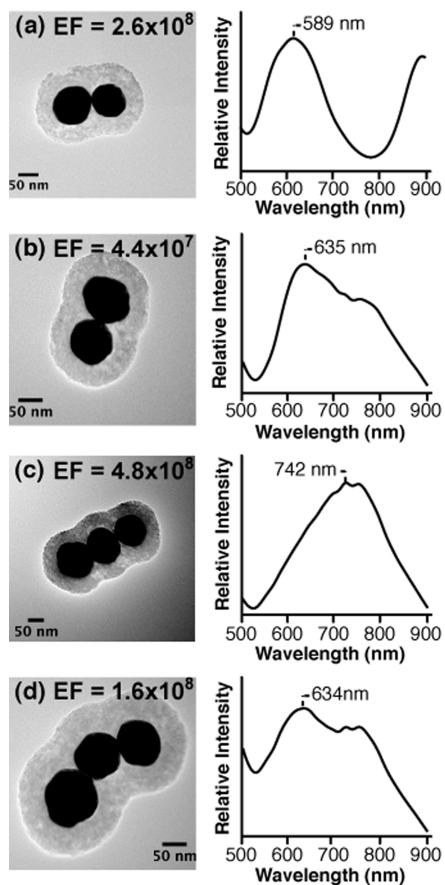


**Figure 4.** Correlated TEM, LSPR, and SERS measurements of dimer and trimer nanoantennas. (a, b) Despite possessing similar structures, dimers exhibit significantly different LSPR spectra, suggesting that variations in gap size play a significant role in determining LSPR. Yet, the EFs are within an order of magnitude. Comparing the dimer in a and the trimer in d shows that addition of more hot spots to the nanoantenna does not result in additional enhancement. Trimer nanoantennas of line (c) and bent (d) geometries have different LSPR spectra but similar EFs. These results show that the nanoantennas exhibit disperse nanostructures and LSPR spectra but relatively constant EFs.

$d_{\text{gap}}$ .<sup>13,14</sup> For example, for a dimer of 100 nm diameter nanoparticles, changing  $d_{\text{gap}}$  from 0.25 to 1 nm resulted in a red shift of the dipole plasmon resonance by more than 200 nm.<sup>16</sup> The data in Figure 4 as well as the broad distribution of single-nanoantenna LSPRs presented in Figure 1b is consistent with a distribution of  $d_{\text{gap}}$  values within the sample. It is therefore quite remarkable that the SERS EFs of the dimers and trimers in Figure 4 are approximately constant, regardless of their diverse structures and LSPRs.

From the data in Figure 4 the role of structure and LSPR in determining EF is yet unclear. The factors that may contribute to the overall enhancement include aggregation state (i.e., number of hot spots),<sup>39</sup> LSPR wavelength,<sup>12</sup> and  $d_{\text{gap}}$ .<sup>13,14</sup> We first considered the effect of aggregation state on EF. A semilogarithmic plot of EF versus aggregation state ranging from dimers to heptamers is presented in Figure 5a. The average EF of 30 single nanoantennas is  $1.0 \pm 0.2 \times 10^8$ , with individual values ranging from  $6.6 \times 10^6$  to  $4.8 \times 10^8$  and the error corresponding to the standard deviation of the mean. The

average EF as a function of aggregation state is  $9.9 \times 10^7$ ,  $1.1 \times 10^8$ ,  $1.7 \times 10^8$ , and  $1.1 \times 10^8$  for dimers, trimers, tetramers, and pentamers, respectively (Figure 5b). Adding more hot spots to the nanoantenna does not increase EF, suggesting that one hot spot dominates the overall enhancement, consistent with the data presented in Figure 3c. In order to test the existence of a relationship between nanoantenna LSPR wavelength and EF, we generated plots of EF versus each of the LSPRs for each nanoantenna and evaluated the Pearson correlation coefficient ( $r$ ). A weak, positive correlation (i.e.,  $r \approx 0.2$ ) was observed between the dipole plasmon resonance wavelength and EF as shown in Figure 5c. For all other LSPRs, no correlation was observed (i.e.,  $r \approx 0$ ). The absence of a correlation between EF and LSPR wavelength does not imply that coupling the laser excitation wavelength to the LSPR is unimportant. Clearly, the observation of SERS requires excitation of the LSPR. Yet, due to the broad LSPR spectra exhibited by hot-spot-containing nanostructures, this resonance condition is met for a wide variety of excitation wavelengths. The presence of a weak correlation between the EF and dipole plasmon resonance wavelength is consistent with their mutual dependence on  $d_{\text{gap}}$ . Previous results have shown that as  $d_{\text{gap}}$  is made smaller, both the dipole plasmon resonance wavelength and EF are increased.<sup>13</sup> Ultimately, for a collection of 30 nanoantennas having diverse aggregation states and LSPRs, the EF varies by less than 2 orders of magnitude.

Finally, the role of interparticle gap size in EM enhancement was investigated using FEM calculations as well as high-resolution TEM (HRTEM) measurements. Previous studies have demonstrated that the distance between metal nanostructures<sup>13,14</sup> as well as crevice sites that form in fused nanoparticles<sup>40–42</sup> significantly impact EM enhancement. Accordingly, the relationship of hot-spot structure and EF was examined by calculating  $\langle |E_{\text{exc}}|^4 \rangle$  as a function of  $d_{\text{gap}}$  (Figure 5d). By changing  $d_{\text{gap}}$  from  $-0.5$  to 1 nm the average EM enhancement at 632.8 nm is modified by roughly 2 orders of magnitude, consistent with the experimentally observed distribution of EFs. This trend is independent of nanoantenna geometry and was observed for a dimer, L-shaped trimer, and line trimer. Moreover, FEM calculations demonstrate that values of  $d_{\text{gap}}$  greater than  $\sim 1$  nm are insufficient to produce the high EM enhancements required to observe SMSERS (i.e.,  $\geq 10^8$ ).<sup>10</sup>

High-resolution TEM (HRTEM) tilt series of SERS nanoantennas were performed in order to image the hot-spot region and experimentally determine  $d_{\text{gap}}$ . However, measuring the structural properties of the entire nanoantenna as well as the interparticle gap size using subsequent TEM and HRTEM tilt series measurements is problematic for two reasons: (1) repeated exposure of nanoantennas to the electron beam caused structural (and optical) changes and (2) measuring the interparticle region is not straightforward for nanoantennas containing two or more hot spots. Therefore, we performed HRTEM measurements on a representative sampling of nanoantennas to establish the range of  $d_{\text{gap}}$  values. Two configurations of the nanoantennas are observed: separated (Figure 6a) and coalesced cores (Figure 6b). In both cases subnanometer structural features that are associated with high EM enhancement are present. For the case of separated cores, values of  $d_{\text{gap}}$  between 0.4 and 1 nm are observed. For coalesced cores, where no physical gap exists (i.e.,  $d_{\text{gap}} < 0$ ), the two crevices formed by fusion of the cores are as small as

(39) Wang, Z. B.; Luk'yanchuk, B. S.; Guo, W.; Edwardson, S. P.; Whitehead, D. J.; Li, L.; Liu, Z.; Watkins, K. G. *J. Chem. Phys.* **2008**, 128, 5.

(40) Moskovits, M.; Jeong, D. H. *Chem. Phys. Lett.* **2004**, 397, 91.  
(41) Garcia-Vidal, F. J.; Pendry, J. B. *Phys. Rev. Lett.* **1996**, 77, 1163.  
(42) Liver, N.; Nitzan, A.; Gersten, J. I. *Chem. Phys. Lett.* **1984**, 11, 449.

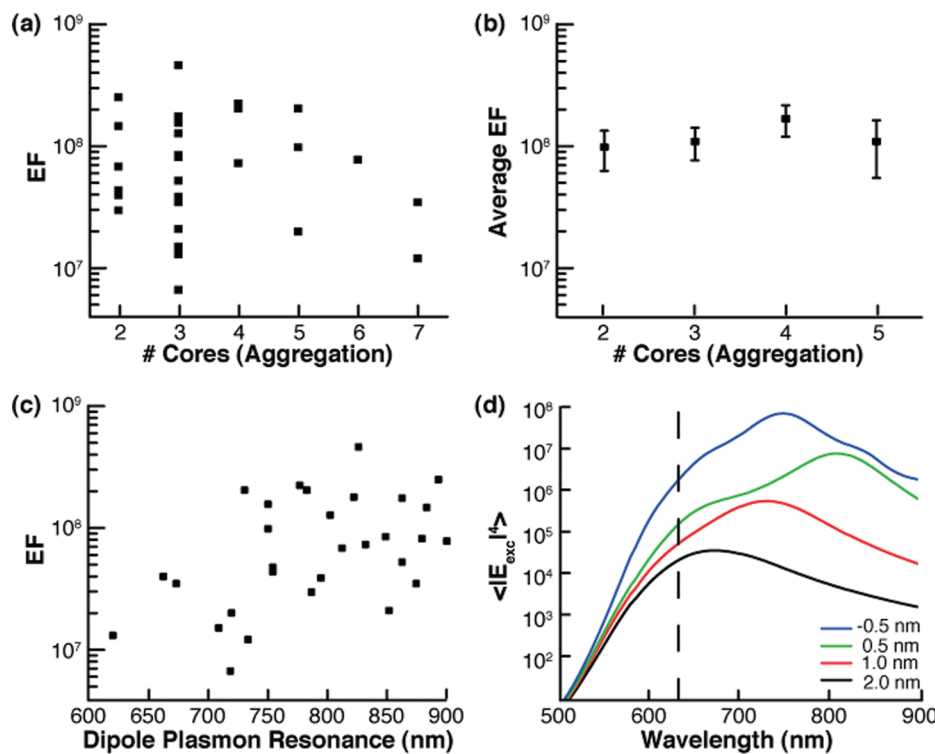


**Figure 5.** (a) Distribution of EFs for 30 SERS nanoantennas as a function of aggregation state ranging from dimers to heptamers. (b) The average EF as a function of aggregation state (where the error bars correspond to the standard deviation of the mean and not the distribution of individual values) is constant with increasing number of hot spots. (c) No correlation is observed between the EF and the dipole plasmon resonance maximum of each nanoantenna. (d) Calculated  $\langle |E_{\text{exc}}|^4 \rangle$  for a dimer nanoantenna showing that the average enhancement is dependent on  $d_{\text{gap}}$ . For 632.8 nm excitation (dashed line), the average EM enhancement varies by approximately 2 orders of magnitude when  $d_{\text{gap}}$  changes from  $-0.5$  (blue line) to  $1$  nm (red line), consistent with the measured EF distribution.

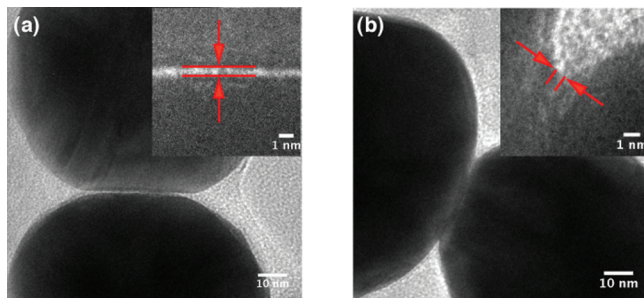


**Figure 6.** HRTEM images of the interparticle regions between Au cores in dimer nanoantennas. (a) Dimer containing a physical gap with a  $d_{\text{gap}}$  of  $\sim 0.4$  nm (inset). (b) Dimer consisting of coalesced cores ( $d_{\text{gap}} < 0$ ), revealing crevices as small as  $0.8$  nm (inset).

0.8 nm. Overall, HRTEM measurements demonstrate that values of  $d_{\text{gap}}$  range from coalescence to  $\sim 1$  nm separation, consistent with the experimentally obtained (Figure 5a) and FEM-calculated (Figure 5d) EF distributions.

## Conclusion

In organic chemistry, structure–activity relationships are widely used to connect molecular architecture to chemical reactivity. However, corresponding studies of hot-spot-containing nanostructures are not as straightforward, due to variations in nanoparticle size, aggregation state, and geometry among members of the ensemble. Here, for the first time, correlated TEM, LSPR, SERS, and FEM studies were performed on a collection of *individual* SERS nanoantennas in order to develop

the detailed structure–activity relationships in hot-spot-containing nanostructures with a precision that has not been achieved by other correlated studies.<sup>21</sup> The average EF for 30 single nanoantennas is  $1.0 \times 10^8$ , with individual values ranging from  $6.6 \times 10^6$  to  $4.8 \times 10^8$ . We find that EFs do not correlate with aggregation state, meaning that a single hot spot between two particles is sufficient, and the “extra” particles are not contributing significantly to the SERS signal. In addition, FEM calculations confirm that the hot spot with the smallest  $d_{\text{gap}}$  dominates the overall enhancement. In contrast to what has been observed for isolated nanoparticles,<sup>12</sup> no direct correlation between LSPR wavelength and EF is observed, consistent with previous investigations of aggregated nanoparticles.<sup>20,43</sup> The presence of a weak correlation between the dipole plasmon resonance wavelength and EF is consistent with their mutual dependence on  $d_{\text{gap}}$ . HRTEM measurements show that the nanoantennas possess interparticle gap sizes within the range of coalescence to  $\sim 1$  nm separation. The EM enhancement at 632.8 nm is modified by roughly 2 orders of magnitude when changing  $d_{\text{gap}}$  from  $-0.5$  to  $1$  nm, consistent with the measured EF distribution. Therefore, whereas the EFs are uncorrelated to the aggregation state and LSPR wavelength, they are crucially dependent on the size of the interparticle gap, as shown by FEM calculations. The ramifications of these findings for the rational design of nanoparticle-based SERS-active materials are significant. A gap is not required to form a hot spot. Molecular recognition-based approaches that bring nanoparticles within *close* but not *intimate* ( $d_{\text{gap}} < 1$  nm) proximity will not lead to structures with maximum

(43) Hoflich, K.; Gosele, U.; Christiansen, S. *J. Chem. Phys.* **2009**, 131, 7.

EFs. Finally, the creation of hot spots, where two nanoparticles are in subnanometer proximity or have coalesced to form crevices ( $d_{\text{gap}} < 0$ ), is paramount to achieving maximum SERS enhancements.

**Acknowledgment.** This research was supported by the AFOSR/DARPA Project BAA07-61 (FA9550-08-1-0221), the NSF (CHE-

0414554 and CHE-0911145), the NSF Network for Computational Nanotechnology, and the NSF MRSEC (DMR-0520513) at the Materials Research Center of Northwestern University. We thank the NUANCE Center at Northwestern University for providing access to the TEM.

JA104174M